SUPPLEMENTARY MATERIALS

1. Detailed data reduction and corrections for $^{14}CO_2$ sublimation samples

1.1. Empirical correction for ANSTO processing

To correct for the effects of graphitization and other processing at ANSTO, we first used a linear empirical correction from commensurately-sized ^{14}C standards (Table S7, Fig. S1). The empirically corrected $^{14}CO_2$ values for the BFI and ice samples are shown in Tables S8-S10.

1.2. Extraneous carbon added from the sublimation procedure

At the end of each sublimation, we calculated the C mass (M_g, mass before graphitization) of the sample by expanding the cryogenically-trapped CO_2 into a calibrated manometer volume. Assuming the [CO_2] measurement in the subsample from OSU (Table S9) is representative of the larger sublimation sample, the expected C mass (M_s, "true" mass of the sample) can be calculated from the amount of air trapped in the molecular sieve. Based on the elevation of the measured C mass (M_g) over the expected C mass (M_s), we calculated that the extraneous C (M_{ext}) introduced by the sublimation system is non-negligible (0.37 ± 0.38 μgC, 2σ, n = 23, Table S9).

We used the laboratory-produced BFI samples to calculate the ^{14}C activity ($^{14}C_{ext}$) of this extraneous C (with mass M_{ext}) added from sample preparation, handling, and sublimation using the following mass balance equations:

$$M_g \cdot {}^{14}C_g = M_s \cdot {}^{14}C_s + M_{ext} \cdot {}^{14}C_{ext} \quad \text{Eq.S1}$$

$$M_g = M_s + M_{ext} \quad \text{Eq.S2}$$

where $^{14}C_g$ is the measured ^{14}C activity after the empirical correction for ANSTO processing (Table S8) and $^{14}C_s$ is the true ^{14}C activity of the CO_2 in the ice sample (corrected for the extraneous C addition from the sublimation system). All ^{14}C terms in Eq. S1 and Eq. S2 are in percent modern carbon (pMC) units, which have been shown to be mass-additive (Petrenko et al., 2008).

For the BFI samples, the "true" ^{14}C activity ($^{14}C_s$) is the $^{14}CO_2$ activity of the standard gas. The expected C mass (M_s) for the BFI samples was calculated from the amount of air trapped in the molecular sieve and the [CO_2] of the standard gas. Using Eq. S1 and Eq. S2, we can solve for $^{14}C_{ext}$ for each laboratory-produced BFI sample. All relevant mass balance variables (M_g, M_s, M_{ext}, $^{14}C_g$, $^{14}C_s$, and $^{14}C_{ext}$) from the laboratory-produced BFI samples are shown in Table S8.

The error-propagated uncertainty of the extraneous carbon ^{14}C activity ($^{14}C_{ext}$) inferred from individual BFI measurements was large, especially in samples that used the modern standard gas because the measured ^{14}C activities of the BFI samples ($^{14}C_g$) were indistinguishable from the "true" ^{14}C activity of the standard gas ($^{14}C_s$). In comparison, for BFI samples that used the ^{14}C-dead standard gas, the measured ^{14}C activities of the blanks were elevated by ~3 pMC compared to the "true" ^{14}C activity of the standard gas (Table S8). This strongly suggests that the main source of the extraneous carbon to the sublimation device is likely CO_2 from ambient air, which has a "modern" ^{14}C signature.

On average, we calculated that $^{14}C_{ext}$ = 125.9 pMC; the standard deviation of $^{14}C_{ext}$ is ± 47.1 pMC (1σ), and the standard error of the mean of $^{14}C_{ext}$ is ±15.7 pMC. We used twice the standard error of the mean (±31.4 pMC) from all 9 laboratory BFI samples as the 2σ uncertainty for $^{14}C_{ext}$ and solved for $^{14}C_s$ in each sample using Eq. S1 (Table S9), assuming the amount of extraneous carbon and its ^{14}C activity from the BFI measurements were representative of the extraneous carbon that was introduced to the samples. This correction represents the biggest source of uncertainty for the $^{14}CO_2$ measurements. Finally, we used TAC from OSU subsamples (Table S9) to convert between $^{14}CO_2$ molecules per cc STP and $^{14}CO_2$ molecules per g ice (Petrenko et al., 2016 Electronic Annex S1).

1.3. Corrections for post-coring in situ ^{14}C

After correcting for the extraneous C added from the sublimation process, the sample ^{14}C values were further corrected for post-coring *in situ* $^{14}CO_2$ production (i.e., $^{14}CO_2$ produced by cosmic rays during storage and transport after the ice samples were brought up to the surface). The post-coring production was constrained by comparing the $^{14}CO_2$ content in field-produced BFI against laboratory-produced BFI (which did not contain the

additional post-coring $^{14}CO_2$, Table S10). We used the ratio of air from the standard gas collected at the end of the sublimation to the mass of BFI that was sublimated as our BFI "air content." We then used this "air content" of the BFI samples and the [CO_2] measured from the manometers to convert the $^{14}CO_2$ measured in the BFI samples into $^{14}CO_2$ molecules per gram of bubble free ice (Table S10). From 4 laboratory-produced BFI samples that used ^{14}C-dead standard gas and 5 field produced BFI samples that used the same standard gas, we calculated that the post-coring ^{14}C production added 8.2 ± 5.9 $^{14}CO_2$ molecules g^{-1} ice (1σ) to the samples (Table S10). The sample $^{14}CO_2$ content after all corrections and the associated propagated uncertainties is shown in Table S9.

1.4. $^{14}CO_2$ analytical uncertainty and acceptance criteria for Monte Carlo method to estimate model parameter uncertainties

The uncertainty of the $^{14}CO_2$ measurements is critical to the interpretation of the data, as it is the largest source of uncertainty for total ^{14}C. The uncertainties of our $^{14}CO_2$ measurements from step-by-step error propagation (Table S8, on average ±31.6 $^{14}CO_2$ molecules/g ice, 95% CI) are comparable to the uncertainty reported in prior studies that used a dry extraction method (van De Wal et al., 2007; van Der Kemp et al., 2002, ~21 $^{14}CO_2$ molecules/g ice). The agreement between replicate samples is, however, much better than what would be expected from the error-propagated uncertainties in individual measurements (Table 1, Table S8). We calculated the pooled standard deviation of replicate pair measurements (s_p) for the $^{14}CO_2$ samples following McNaught and Wilkinson (1997)

$$s_p = \sqrt{\frac{\sum(x_{i1} - x_{i2})^2}{2k}} \qquad \text{Eq.S3}$$

where x_{i1} and x_{i2} refer to measurement #1 and measurement #2 from depth interval *i* and *k* refers to the number of replicate pairs. The uncertainty derived from pooled standard deviation of replicate pair measurements (±12.4 $^{14}CO_2$ molecules/g ice, 2σ) is notably lower than the error-propagated uncertainties (±31.6 $^{14}CO_2$ molecules/g ice on average, 95% CI). The pooled standard deviation is even lower (±7.8 $^{14}CO_2$ molecules/g ice, 2σ) if

we exclude the replicate pair from 2.25 m depth. The shallow (< 6m) ice in Taylor Glacier has been shown to contain ambient air contamination from near-surface thermal contraction cracks (Baggenstos et al., 2017; Petrenko et al., 2016). These thermal cracks are not homogenous, can heal, and become invisible to the naked eye. Despite being collected from the same depth, the two 2.25 m samples might contain different amounts of ambient air.

Both methods of determining analytical uncertainties (error-propagation vs. pooled standard deviation from replicates) are in principle valid. For the $^{14}CH_4$ and ^{14}CO measurements, we used the error propagation method because we do not have replicates. When replicate measurements are available, it is common practice in ice core analysis to use the pooled standard deviation (e.g., Mitchell et al., 2013). Based on the observation that the ratios of $^{14}CO_2$ to other ^{14}C species (Fig. S4B, Section 4.2) are relatively constant, it is likely that the error propagation method overestimates the uncertainty of our $^{14}CO_2$ measurements.

However, when we use the smaller uncertainty from the pooled standard deviation, the ice flow/^{14}C production model was not able to produce a total ^{14}C profile that can fit all measurements within their 95% CI uncertainties (Fig. 6b). The best-fit ^{14}C profile from the model fell outside the 95% CI uncertainties of total ^{14}C from two depth ranges (10 m and 72 m samples). The samples from these two depth ranges show excellent agreement among their replicates (Table 1, Fig. 6b); there were also no analytical issues that would call these values into question. If the analytical uncertainty of the $^{14}CO_2$ data is truly ±31.6 $^{14}CO_2$ molecules/g ice (95% CI), it is very unlikely that the combined data (^{14}CO, $^{14}CO_2$, and $^{14}CH_4$) can produce the observed $^{14}CO_2$/total ^{14}C ratio of 0.66 ± 0.12 (95% CI, Table 1, Fig. S4B).

One possible explanation for the model-data mismatch at 10 m and 72 m depth ranges is that because of their smaller sample size, the $^{14}CO_2$ samples might be more susceptible to small-scale variations in ice flow that are not captured by the 2D ice-flow model. For example, heterogeneity in ice rheology may play a role. Our samples (from 0 to 72m depth) span a large range of ages (50-92 kyr BP), over several Dansgaard-Oeschger events and

Marine Isotope Stages. As such, they have significantly different impurity content and ice with higher chemical impurities deforms more easily (Stoll et al., 2021). Marine Isotope Stage 4 (MIS4) ice (~55-72 kyr BP), which is characterized by high dust content (Menking et al., 2019) was missing entirely in the cores we drilled (Section 3 of Supplementary Materials). MIS4 ice was also missing from the Taylor Glacier across-flow transect (Baggenstos et al., 2017) but it does outcrop several hundred meters downglacier (Menking et al., 2019; Shackleton et al., 2021). This shows that there is preferential deformation of dusty ice in Taylor Glacier (which might account for why $^{14}CO_2$ values from certain depth ranges show excellent agreement among replicates but are off from the model-predicted ^{14}C) that is not accounted for by the 2D flow model.

Alternatively, it is also possible that the real analytical uncertainty of the $^{14}CO_2$ measurements might be somewhere between the uncertainties estimated via the error-propagation and pooled standard deviation methods. There can be additional sources of uncertainties that are not captured by pooled standard deviation among replicates. For example, processes such as gas loss (especially for the deeper samples) can affect both replicate samples equally and bias the signal. Furthermore, as we are working with a relatively small dataset, the pooled standard deviation among the 9 pairs of replicate measurements might underestimate the analytical uncertainty of the system. More measurements of ice with known exposure history, age, and more sample replicates are needed to better constrain the overall analytical uncertainty of the sublimation system for $^{14}CO_2$ measurements. However, there are also sources of uncertainties in the sublimation system that do not contribute to the overall variability (and thus precision) the analytical measurements. For example, the determination of air content and $[CO_2]$ of the sublimation samples are based on pressure readings with volume-calibrated manometers. Both the pressure gauge readings and the manometer volumes have uncertainties that are propagated through the overall uncertainties with the step-by-step error propagation method. However, the manometer volumes do not change from sample to sample, and thus this kind of uncertainties do not contribute to measurement variability and not accounted by the pooled standard deviation of replicates (which is ultimately a measure of analytical precision).

We argue that the uncertainty derived from pooled standard deviation method is more appropriate to use for our case. We used the pooled standard deviation (±7.8 $^{14}CO_2$ molecules/g ice, 2σ) as the uncertainty for all $^{14}CO_2$ measurements except the 2.25m sample pair, which are affected by modern air contamination from surface cracks (where we used the error-propagated uncertainties instead, Table 1). However, considering that the model was not able to fit all the data at 95% CI uncertainty even with the best-estimate model parameters (σ_0, f_{tot}, and flow trajectories), it is not surprising that the Monte Carlo simulations also struggle to find a pair of σ_0 and f_{tot} that can fit all measurements within their 95% CI. An alternative acceptance criteria to estimate the uncertainties of the ^{14}C production model parameters is needed. In the Monte Carlo method, we accept all model parameters (σ_0 and f_{tot}) that produce model-calculated, total ^{14}C within the 95% CI and 68% CI measurement uncertainties of the total ^{14}C from the best-fit parameter values (Fig. 6, Fig, 7). This approach essentially cancels out the representation error from the ice flow/^{14}C production model and provides uncertainty estimates for σ_0 and f_{tot} that are based solely on the prescribed analytical uncertainties.

2. Subsample [CH_4] measurements and sample integrity of the large volume samples

The [CH_4] measurements from continuous flow analysis (CFA) on TG-Deep3 core (borehole #3) and the [CH_4] from the large volume samples (which combine ice from all three boreholes) are shown in Fig. S9. The continuous [CH_4] measurements show high variability near the ice surface. The near-surface elevation in [CH_4] is likely because of contamination from modern air due to thermal cracks (Baggenstos et al., 2017; Petrenko et al., 2016) and the depletion is likely due to consumption of CH_4 by methanotrophic microbes. The $\delta^{13}CH_4$ value of Taylor Glacier surface sample is ~10‰ higher relative to typical atmospheric $\delta^{13}CH_4$ values of -47‰ (Table S1), indicating likely biological fractionation during methane consumption. Alterations of trace gases in the shallowest ice at margin sites are common and not unique to Taylor Glacier (Petrenko et al., 2006; Turney et al., 2013). The ^{14}CO and $^{14}CH_4$ measurements from the "surface" sample are thus also rejected.

Another stand-out feature in the CFA data is the low [CH_4] values between ~24-27 m depth (Fig. S9). Discrete [CH_4] measurements from the gas chromatography (GC) system (Mitchell et al., 2011) were conducted to rule out the possibility of instrument error from the CFA system. The discrete measurements confirmed the validity of the CFA measurements and furthermore showed unusual reduction in total air content (TAC) of the ice in this low-[CH_4] section. The [CH_4] values observed in this section (200-300 nmol/mol) are lower than the lowest observed atmospheric [CH_4] over the past 800 kyr (Loulergue et al., 2008), and thus the possibility that the low CH_4 section represents an ice section from another time period can be ruled out. In this core section we do not have strong evidence for microbial consumption; unlike the surface samples, the $\delta^{13}CH_4$ values in the large volume samples adjacent to this section (19.5m and 30m) are within the range of glacial-interglacial variability (Table S1). Additional measurements of $\delta^{13}CO_2$ and $\delta^{13}CH_4$ would be useful to investigate the microbial consumption hypothesis. The ^{14}CO and $^{14}CH_4$ in the 19.5m large volume sample from 2015/16 were rejected because the samples partially contained ice from this section.

The [CH_4] from the "30m" large volume sample is also strongly elevated relative to the CFA measurements. This sample also contains unusually elevated CO (Table S5) and highly chlorinated compounds measured by the SIO GC-MS system (not shown). However, this contamination is likely unrelated to the anomalous [CH_4] depletion observed by the CFA measurements around this region. Instead, during the on-field processing of this sample at Taylor Glacier, we encountered a problem with the electric bandsaw that was usually used to cut the CFA "stick" subsamples (Fig. S1). The CFA "sticks" for the 30m sample were instead cut with an electric chainsaw (which was significantly dirtier than the electric bandsaw). Thus, the anomalous elevation of [CH_4] on the 30m sample was likely due to contamination from the electric chainsaw. Because of this contamination, the 30m sample results are rejected.

The 40.5m, 51m, and 61.5m large-volume samples also show slightly elevated [CH_4] relative to the CFA measurements, although not to the extent of the 30m sample (Fig. S9). Unlike the 30m sample, the 40.5m, 51m, and 61.5m sample do not contain anomalously

high CO or chlorinated compounds. For these samples, the discrepancy between the [CH_4] measurement from the bulk large volume sample and CFA subsamples is likely be due to slight age offsets between the boreholes (only borehole #3 was subsampled and measured with CFA system).

3. Sample age determination and integrity of $^{14}CO_2$ samples

The age-scale for the samples used in this study was established via matching the measured CFA [CH_4] from the continuous subsample sticks onto other ice core records with well-established chronologies. The continuous [CH_4] from TG-Deep3 was matched to the continuous [CH_4] from the NEEM (North Greenland EEMian Ice Drilling) ice core (Chappellaz et al., 2013) using manually picked tie points. From the CH_4 synchronization, it is clear that the samples used in this study are all older than 55 ka (Fig. S10). Thus, we do not expect any ^{14}C inheritance from the accumulation site.

We also compared the measured [CO_2] in our samples to [CO_2] from other Antarctic ice cores (Bereiter et al., 2015) to confirm the integrity of the $^{14}CO_2$ samples. However, for a direct comparison with existing CO_2 records, we have to transfer the TG-Deep3 / NEEM gas age scale onto the AICC12 (Antarctic Ice Core Chronology) age scale (Veres et al., 2013). Currently the NEEM gas age is not included in AICC12. However, in the GICC05 (Greenland Ice Core Chronology) framework (Rasmussen et al., 2006; Rasmussen et al., 2013) the NEEM ice age is synchronized with NGRIP ice age (North Greenland Ice Core Project). NGRIP ice and gas age were included in AICC12 (Veres et al., 2013). This allows us to transfer our TG-Deep3/NEEM gas age onto AICC12 gas age by first interpolating the TG-Deep3(NEEM) gas age onto NEEM & NGRIP ice age and then onto NGRIP/AICC12 gas age.

The [CO_2] measurements from our samples agree well with [CO_2] from EDML ice core, except for the "30m" sample (~72 ka) which has a significantly lower [CO_2] than the Antarctic ice core composite (Fig. S10). As discussed above, at this depth the [CH_4] is also anomalously depleted (Fig. S9), and the [CO] in the large volume sample is anomalously

elevated (Table S5). This depth range is also associated with a large age discontinuity (Fig. S9). The "30m" $^{14}CO_2$ sample was thus rejected.

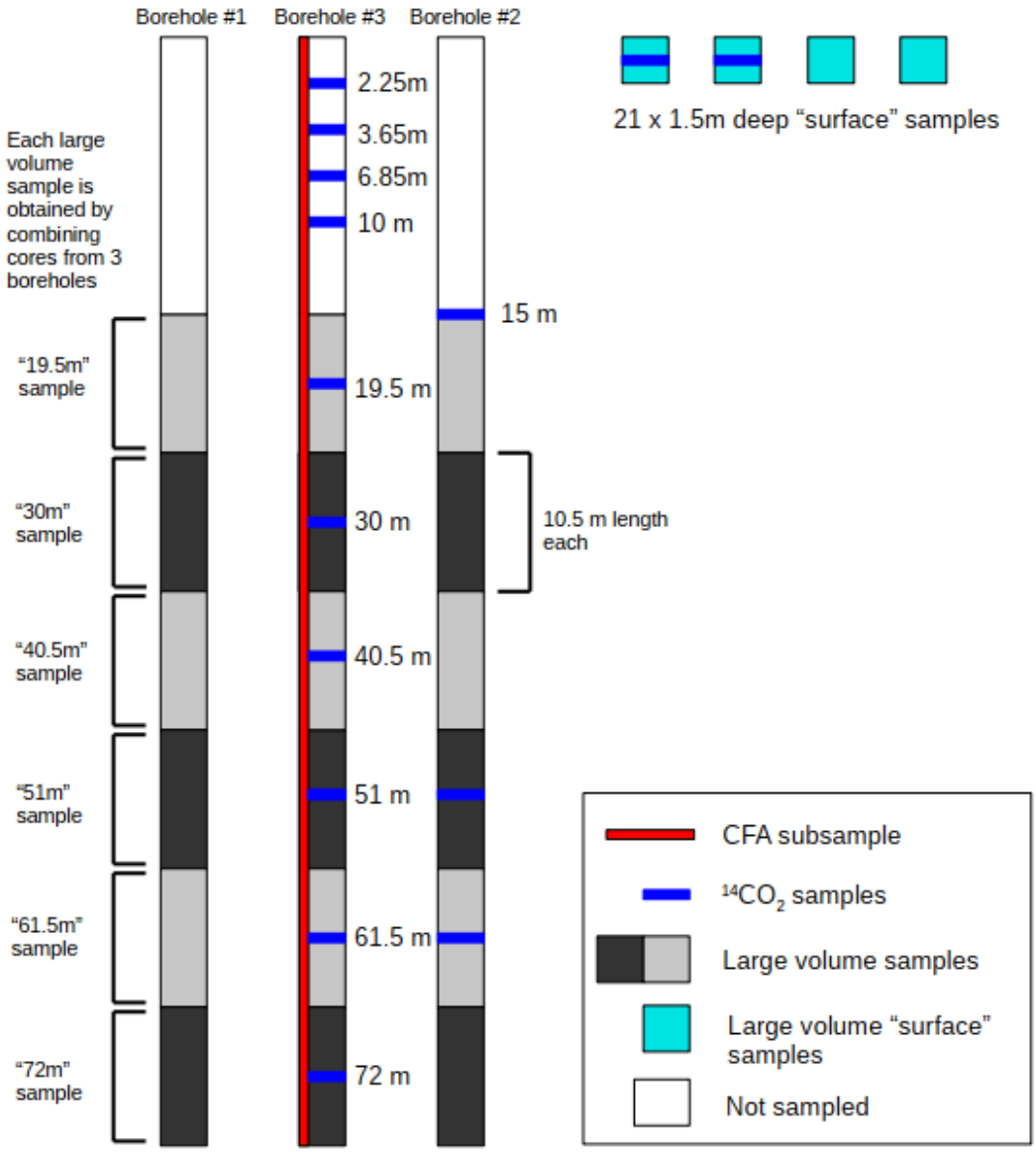

Fig. S1. Sampling scheme for the Taylor Glacier 2015/2016 field season ^{14}C samples. Each large-volume sample for $^{14}CH_4$ and ^{14}CO measurements requires ~1000kg of ice. For the deep samples (>19.5 m, shown in light and dark grey), this is achieved by combining same depth samples from 3 Blue Ice Drill (BID) boreholes, 10.5 m in length from each borehole. For the "surface" large-volume sample (shown in light blue), we combined 21 surface BID ice cores, 1.5 m length each into one large-volume sample. 3x3 cm CFA "stick" subsamples (shown in red) were cut from the whole length of borehole #3 for age control. 2-3 kg discrete samples for $^{14}CO_2$ measurements (shown in dark blue) were taken from the large-volume mid-depths of borehole #3 and borehole #2. Additional discrete $^{14}CO_2$ samples were taken from the mid-depths of Petrenko et al. (2016) large-volume samples (2.25-15 m) to complement their ^{14}CO and $^{14}CH_4$ measurements.

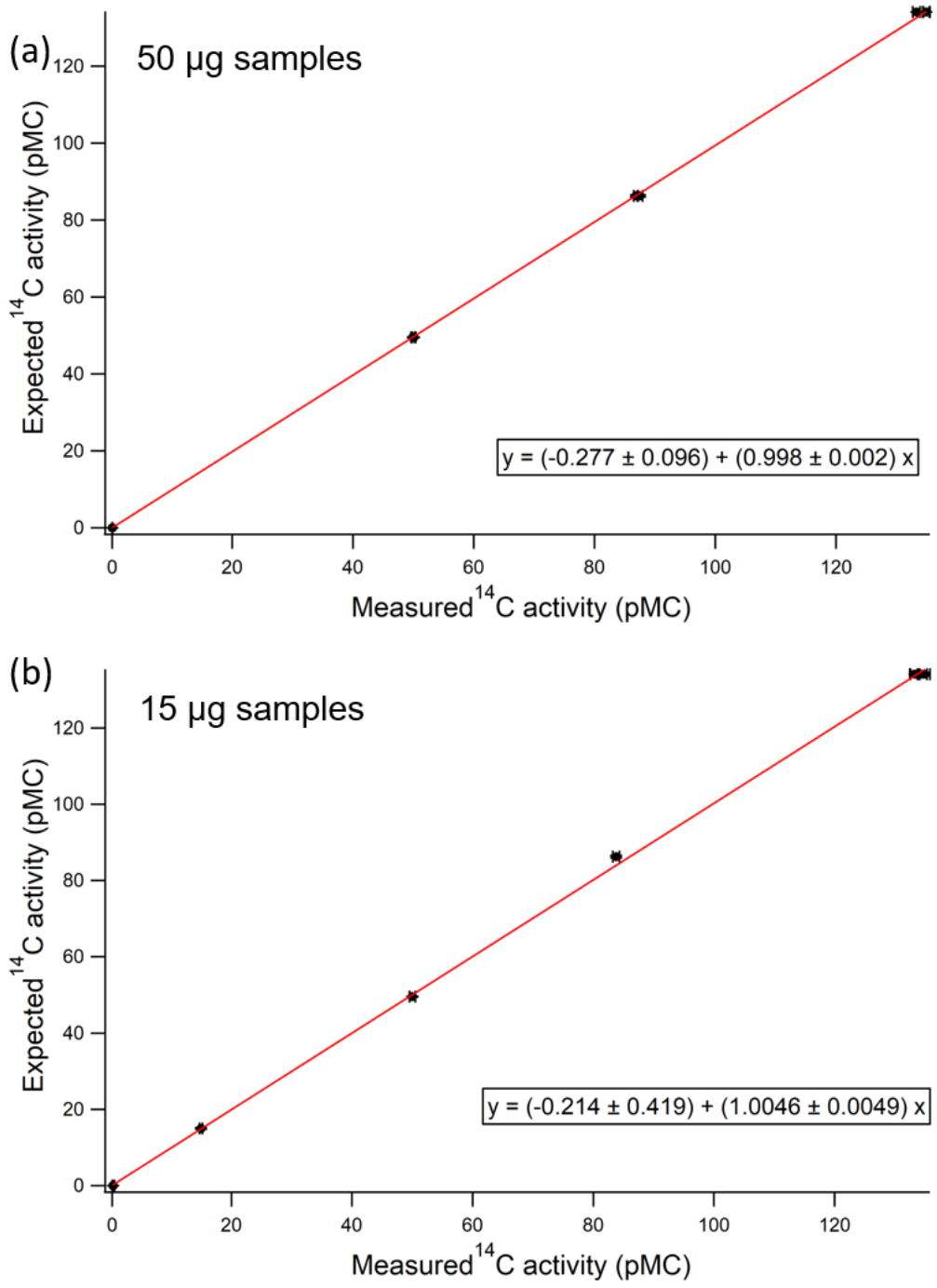

Fig. S2. Linear empirical correction from commensurately-sized ^{14}C standards for the (a) ^{14}CO samples and (b) $^{14}CO_2$ samples. The errors on the coefficients represent 68% CI (1σ). The measured and expected ^{14}C activities of these standards are shown in Table S7.

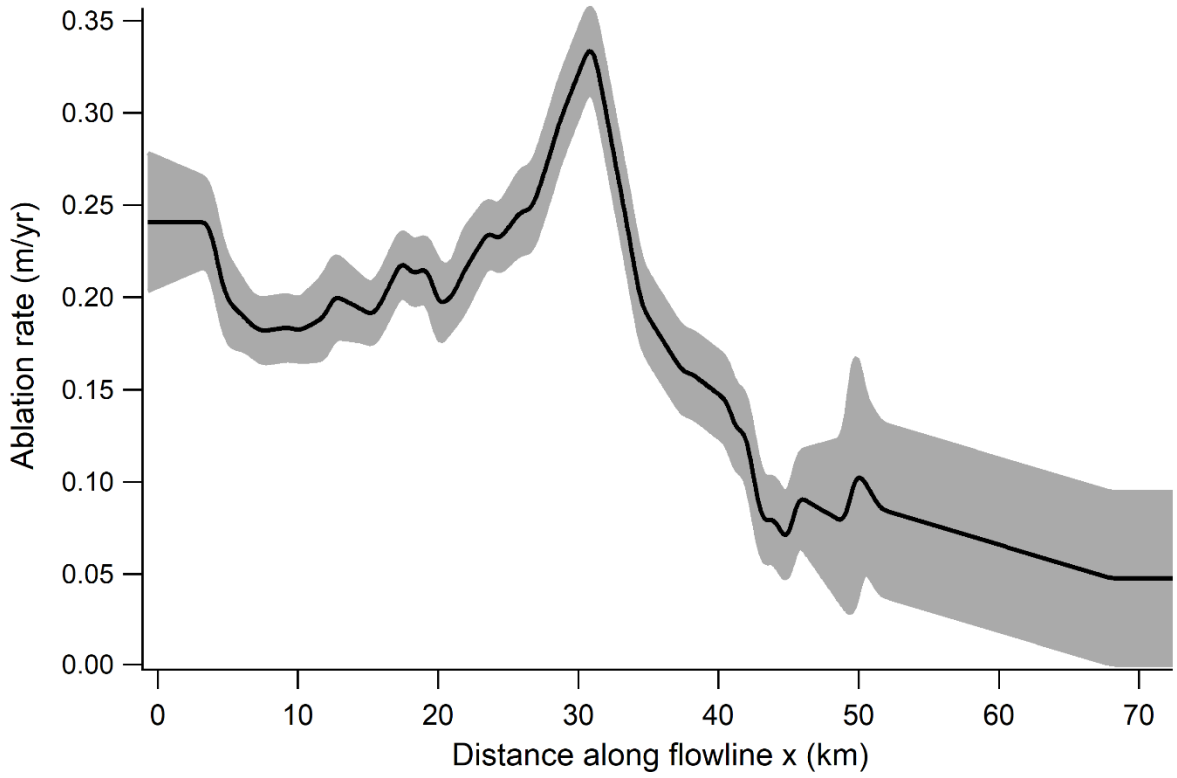

Fig. S3. Ablation rates along the glacier inferred from survey pole data. The shaded region represents 2σ uncertainties.

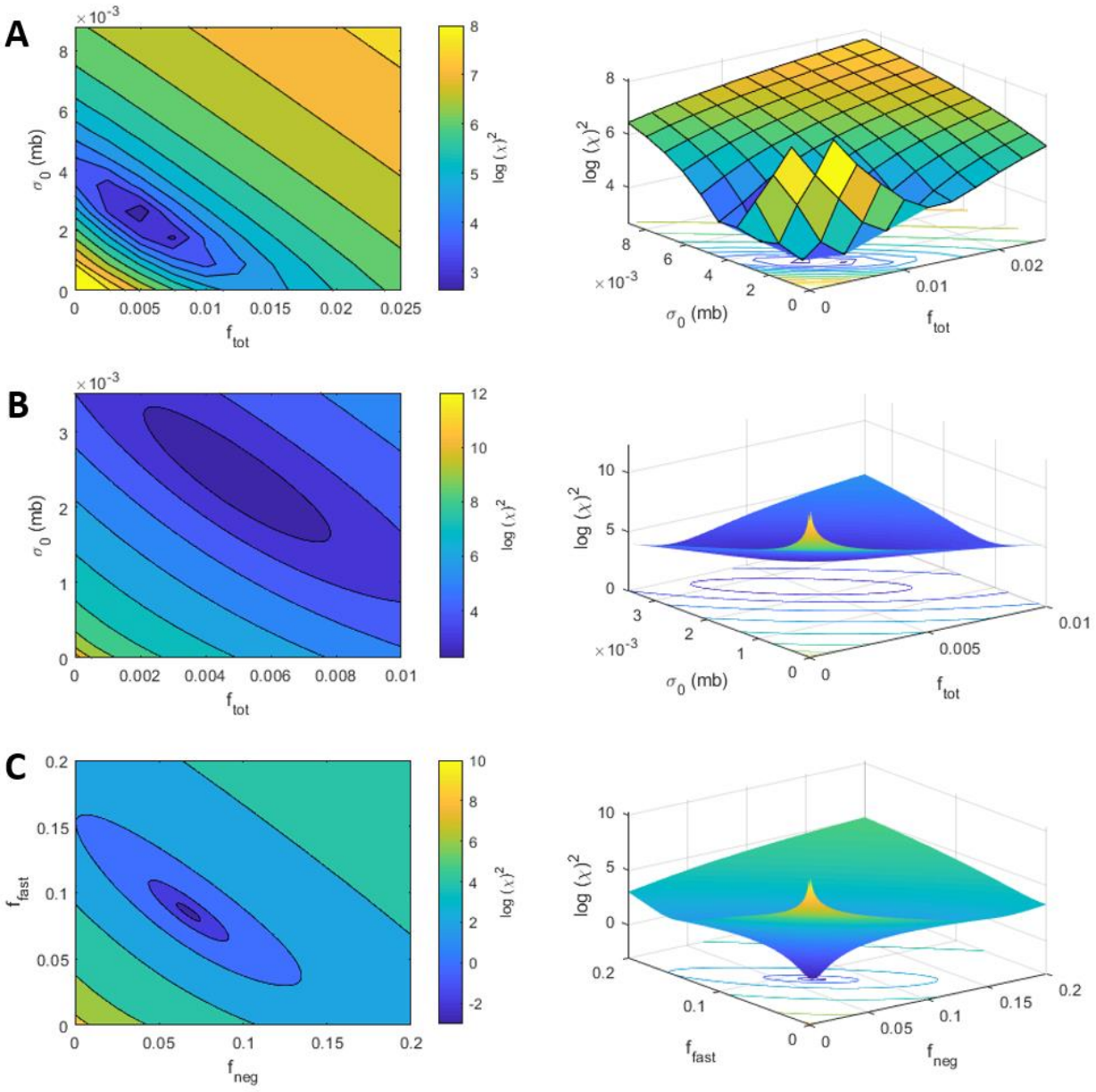

Fig. S4. (A). Goodness of the fit (χ^2) for the coarse grid-search under best-estimate ablation rate scenario to find best-estimate f_{tot} and σ_0. (B). Goodness of the fit (χ^2) for the high-resolution grid-search under best-estimate ablation rate scenario to find best-estimate f_{tot} and σ_0. (C). Goodness of the fit (χ^2) under best-estimate ablation rate scenario to find best-estimate f_{neg} and f_{fast} for ^{14}CO-specific muogenic production rates

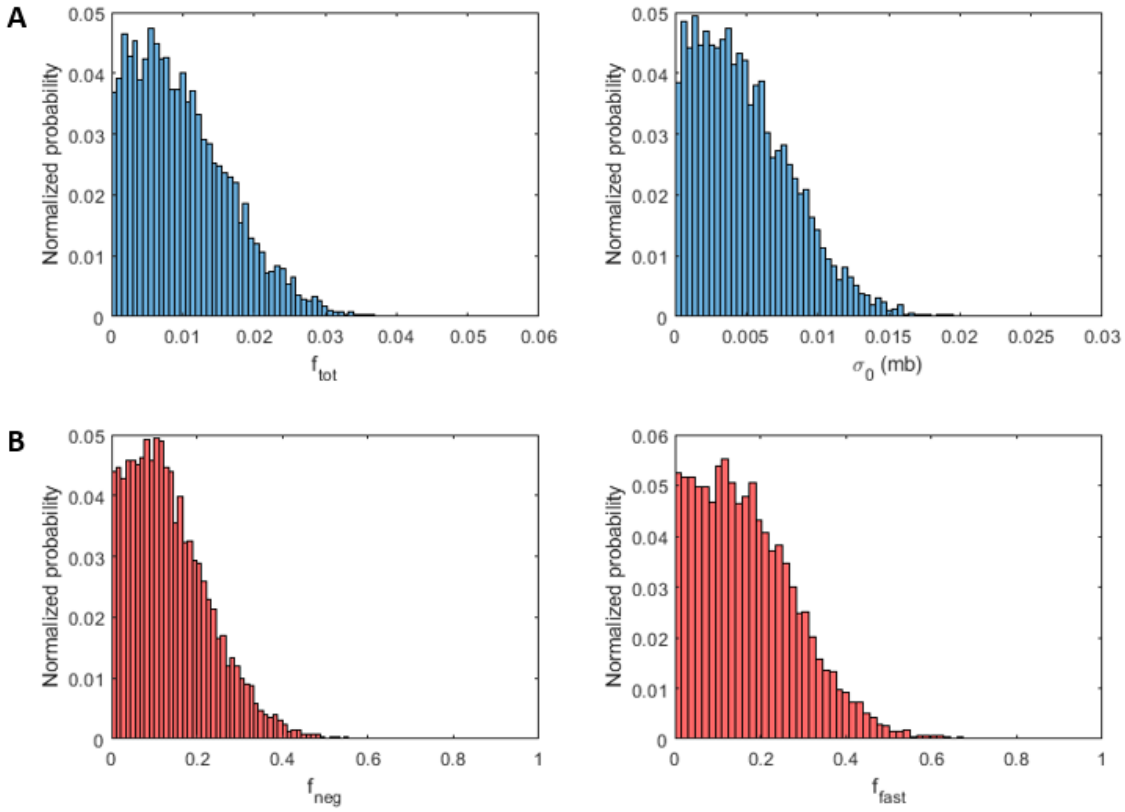

Fig. S5. (A). Prior distribution of model parameters f_{tot} and σ_0 for total ^{14}C production used in the Monte-Carlo simulations to estimate total muogenic ^{14}C production rates. (B). Prior distribution of model parameters f_{neg} and f_{fast} used in the Monte-Carlo simulations to estimate ^{14}CO-specific muogenic production rates.

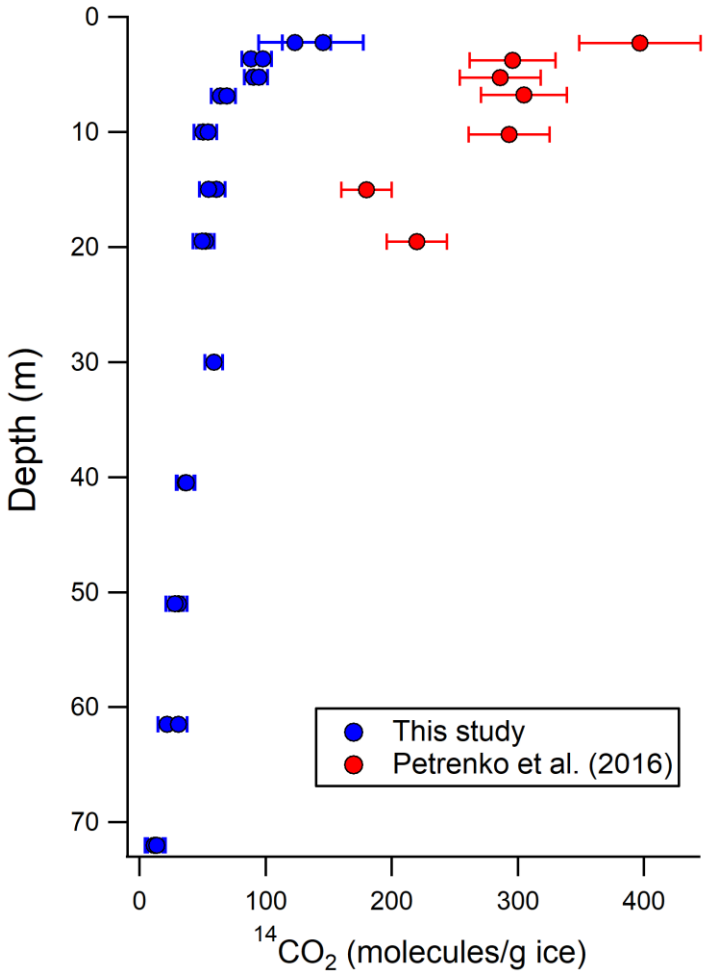

Fig. S6. Comparison between sublimation-based $^{14}CO_2$ measurements (this study) and melt-extraction based $^{14}CO_2$ measurements from Petrenko et al. (2016). Both dataset are obtained from the same site (Taylor Glacier, Antarctica).

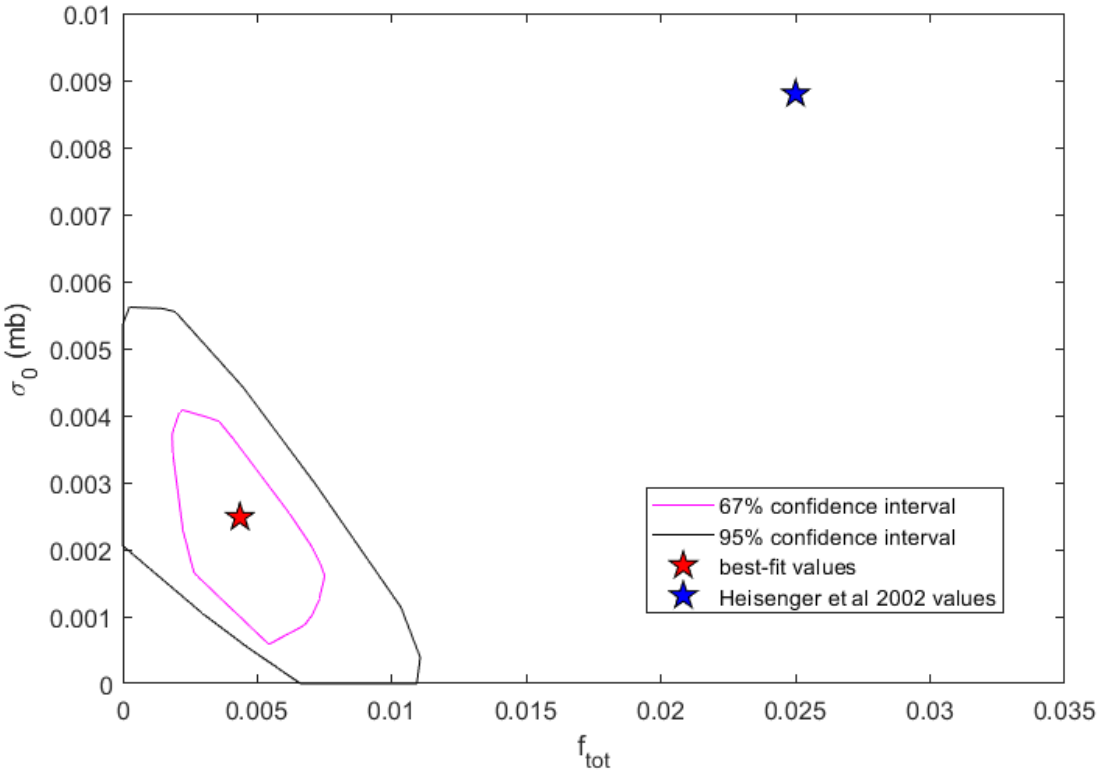

Fig.S7. 68% and 95% CI contours of accepted σ_0 and f_{tot} values for total ^{14}C when the ±31.6 $^{14}CO_2$ molecules/g ice, 95% CI uncertainty from step-by-step error propagation method was used for the $^{14}CO_2$ data as the Monte Carlo acceptance criteria. Even when using the larger and likely overestimated $^{14}CO_2$ uncertainty, our data still clearly show what the Heisinger et al. (2002a, 2002b) values are overestimated.

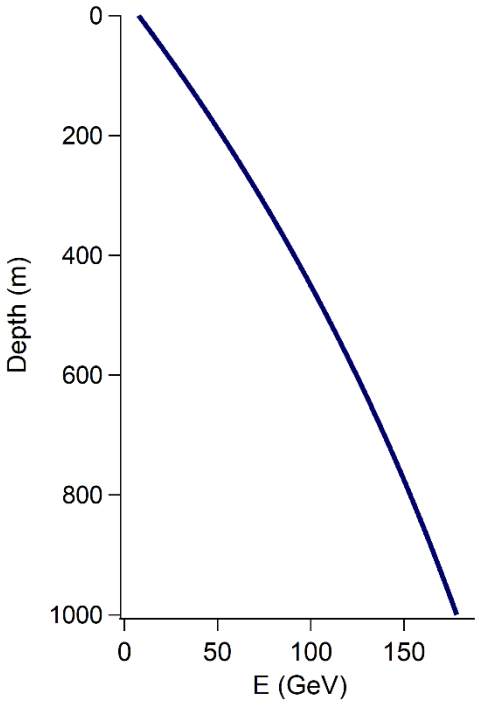

Fig. S8. Calculated mean muon energy ($\bar{E}$) versus depth at Taylor Glacier from Balco et al. (2008) cosmogenic nuclide production model.

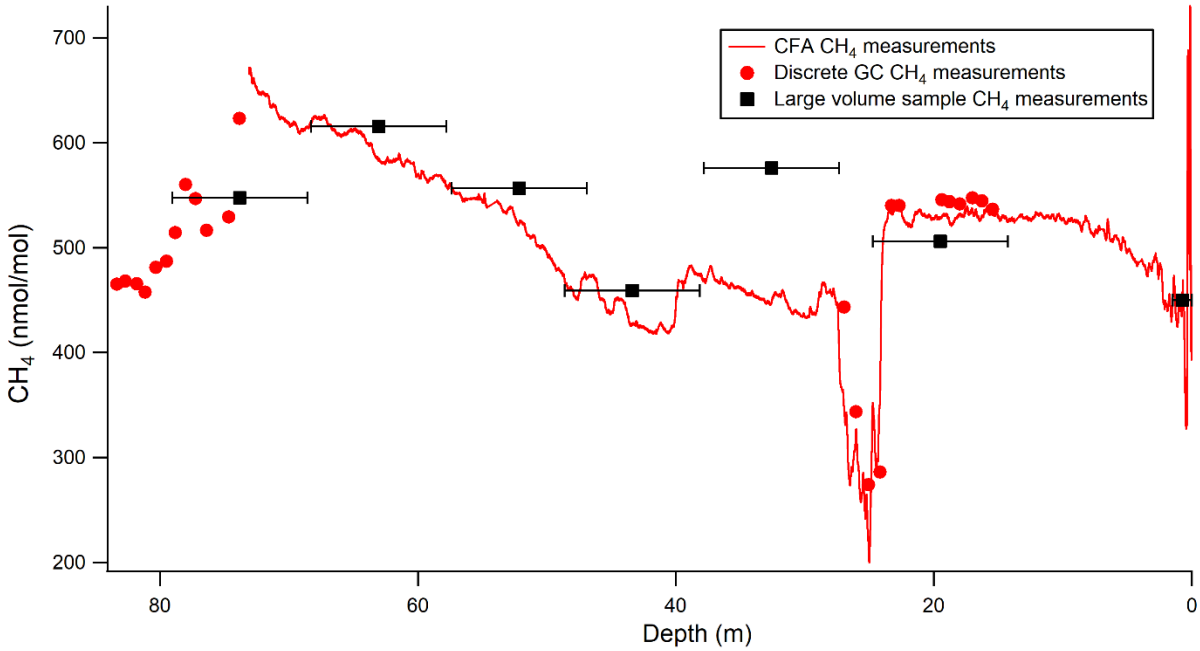

Fig. S9. Depth profile of "TG-Deep3" [CH_4] measurements from CFA, discrete measurements using a GC-FID system, and [CH_4] measurements from large volume samples. The large volume samples combine ice from all three 2015/16 deep boreholes. The horizontal error bars illustrate the depth span of the large volume samples.

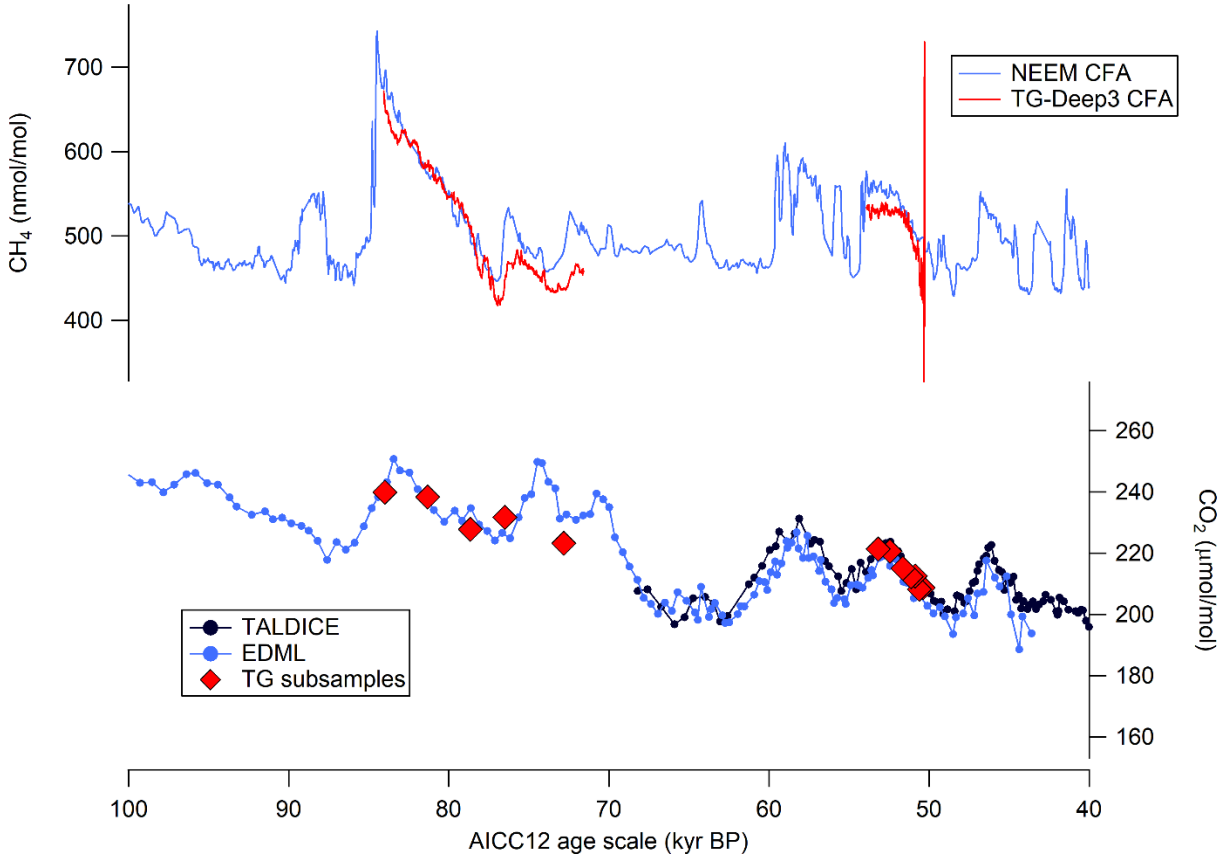

Fig. S10. Continuous flow analysis (CFA) [CH_4] from "TG-Deep3" core (this study), CFA [CH_4] mole fraction from NEEM (Chappellaz et al., 2013), [CO_2] from $^{14}CO_2$ samples used in this study, and composite Antarctic ice core [CO_2] (Bereiter et al., 2015). All data are plotted onto the synchronized AICC12 gas age (Veres et al., 2013).

Table S1. $\delta^{13}C$ measurements on the large volume samples. All errors presented indicate the 95% confidence interval.

Sample name	$\delta^{13}CH_4$ (‰)
Sfc sample	-34.7 ± 0.2
19.5m	-45.1 ± 0.2
30m	-46.8 ± 0.2
40.5m	-47.9 ± 0.2
51m	-48.1 ± 0.2
61.5m	-47.9 ± 0.2
72m	-47.2 ± 0.2

Table S2. Measured CH_4 mole fraction in the large volume samples, field procedural blanks, and associated corrections. All errors presented indicate the 95% confidence interval.

Sample name	CH_4 measured (nmol/mol)	CH_4 solubility correction factor	CH_4 solubility corrected (nmol/mol)	Fraction ultrapure air remaining	Final CH_4* (nmol/mol)
SFC	433.7 ± 0.6	1.034 ± 0.007	448.4 ± 3.0		442.3 ± 3.9
19.5m	495.6 ± 0.4	1.030 ± 0.006	510.2 ± 2.9		504.2 ± 3.9
30m	564.5 ± 0.3	1.028 ± 0.005	580.2 ± 3.1		574.2 ± 4.0
40.5m	450.6 ± 0.6	1.029 ± 0.006	463.5 ± 2.6		457.5 ± 3.7
51m	544.1 ± 0.3	1.030 ± 0.006	560.5 ± 3.3		554.5 ± 4.2
61.5m	600.5 ± 0.5	1.031 ± 0.006	619.1 ± 3.7		613.1 ± 4.5
72m	532.3 ± 0.7	1.035 ± 0.007	551.0 ± 3.8		545.0 ± 4.7
^{14}C dead blank 1	461.9 ± 0.4	1.036 ± 0.007	478.6 ± 3.3	0.0306 ± 0.0253	493.8 ± 13.4
^{14}C dead blank 2	463.4 ± 0.3	1.035 ± 0.007	479.6 ± 3.2	0.0307 ± 0.0256	494.9 ± 13.5
^{14}C modern blank 1	462.3 ± 0.3	1.034 ± 0.007	478.1 ± 3.1	0.0201 ± 0.0018	487.9 ± 3.3
^{14}C modern blank 2	452.8 ± 0.4	1.030 ± 0.006	466.5 ± 2.7	0.0415 ± 0.0139	486.7 ± 7.6
^{14}C dead std gas	498.3 ± 4.6				
^{14}C modern std gas	492.8 ± 3.5				

**the CH_4 mole fraction in the ice samples was further corrected for the 6.0±1.3 nmol/mol melting blank. The numbers shown here include the melting blank correction*

Table S3. Pressure measurements and total air content (TAC) for the large volume samples. All errors presented indicate the 95% confidence interval. For the "30m" sample (marked with an asterisk*), the water level (and thus water volume) was not recorded for 1 (out of 3) melt-extractions. We thus assumed that the water volume for this extraction was equal to the average of all the other extractions for the field season and doubled the uncertainty. We used the SIO pressure measurements for TAC calculation, except for the "51m" sample (marked with two asterisks **) where UR pressure measurement is higher than the SIO pressure measurement, indicating a problem with the recorded SIO measurement. From the average pressure measurement differences within tanks, we assumed that the GC-MS and noble gas measurements at SIO consumed 221 ± 14 torr (95% CI), and used the UR pressure measurement, corrected for sample consumption at SIO, to calculate the TAC. All pressure measurements were taken at room temperature. On average (n=7), the SIO room temperature was 22.0 ± 0.1°C and the UR room temperature was 21.7 ± 0.2°C.

Sample name	SIO pressure corrected for vapor pressure (torr)	UR pressure corrected for vapor pressure (torr)	Pressure difference (SIO-UR) (torr)	Pressure used for air content calculation (torr)	Volume of air extracted (L STP)	Fraction of air in the headspace	Volume of ice extracted (water equivalent, L)	Total air content (cc STP / g ice)
SFC	2533 ± 20	2306 ± 18	227 ± 27	2533 ± 20	117.4 ± 3.9	0.956 ± 0.008	1188 ± 45	0.0989 ± 0.0050
19.5m	2156 ± 17	1927 ± 15	229 ± 23	2156 ± 17	99.7 ± 3.2	0.960 ± 0.007	1168 ± 45	0.0855 ± 0.0043
30m	2325 ± 19	2109 ± 17	216 ± 25	2325 ± 19	107.1 ± 3.5	0.962 ± 0.007	1154 ± 69*	0.0930 ± 0.0064
40.5m	2316 ± 19	2107 ± 17	209 ± 25	2316 ± 19	106.9 ± 3.5	0.961 ± 0.007	1160 ± 44	0.0922 ± 0.0046
51m	*2146 ± 17*	*2227 ± 18*	*-81 ± 25***	*2448 ± 35***	109.3 ± 4.6	0.960 ± 0.007	1163 ± 45	0.0941 ± 0.0054
61.5m	2391 ± 19	2171 ± 17	219 ± 26	2391 ± 19	110.5 ± 3.6	0.959 ± 0.008	1170 ± 45	0.0946 ± 0.0047
72m	2513 ± 20	2289 ± 18	224 ± 27	2513 ± 20	116.6 ± 3.9	0.954 ± 0.008	1193 ± 46	0.0979 ± 0.0050
		Average (n = 6)	221					
		2x standard deviations	14					

Table S4. Measurement of noble gases ($\delta Xe/N_2$, $\delta Kr/N_2$, and $\delta Xe/Kr$) from the field procedural blanks. The large-volume samples are affected by anomalously increased gas solubility relative to the actual measured headspace pressure (P_{head}) due to rising gas bubbles during ice melting and the air recirculation step (which effectively increases the pressure of gas, $P_{exchange}$; see Petrenko et al., 2016). To constrain gas solubility, the ^{14}C-modern standard used in the field procedural blanks was spiked with artificially high Xe and Kr (Dyonisius et al., 2020). We measured the two field procedural blank samples (which undergo a similar air recirculation step as the samples) derived from this standards gas for $\delta Xe/N_2$, $\delta Kr/N_2$, and $\delta Xe/Kr$ relative to the standard gas and estimated the parameter alpha (α), which effectively accounts for the ratio of $P_{exchange}/P_{head}$. Alpha (α) is chosen to minimize the discrepancy between expected $\delta Xe/Kr$ vs. measured $\delta Xe/Kr$ for both modern ^{14}C field procedural blank samples.

Sample name	**Field ^{14}C modern test 1**	**Field ^{14}C modern test 2**
Tank #	SIO15	SIO18
$\delta(Xe/N_2)$, ‰ vs. CB10270 (modern ^{14}C std)	-202.1	-210.3
$\delta(Kr/N_2)$, ‰ vs. CB10270 (modern ^{14}C std)	-95.0	-131.5
$\delta(Xe/Kr)$, ‰ vs. CB10270 (modern ^{14}C std)	-95.0	-90.7
Constants and physical measurements for gas solubility calculation		
Water T during recirculation, K	282.3	279.6
Kr solubility constant (K_h) @ water T, M/atm	0.003573991	0.003820178
Xe solubility constant (K_h) @ water T, M/atm	0.006504131	0.007025663
Headspace volume, L	400	371
Headspace T, K	270	299
Mole fraction under Henry's Law		
Mole fraction of Xe in water	0.182	0.167
Mole fraction of Xe in headspace	0.818	0.833
Mole fraction of Kr in water	0.109	0.098
Mole fraction of Kr in headspace	0.891	0.902
$\delta(Xe/Kr)$ predicted under full eq, ‰	-82.0	-76.0
Mole fraction under increased gas solubility due to recirculation step		
α, tuneable parameter for $P_{exchange}/P_{head}$	1.221	1.221
Mole fraction of Xe in water, with α	0.214	0.196
Mole fraction of Xe in headspace, with α	0.786	0.804
Mole fraction of Kr in water, with α	0.130	0.117
Mole fraction of Kr in headspace, with α	0.870	0.883
$d(Xe/Kr)$ tuned with α, ‰	-96.2	-89.5
δ(Xe/Kr) final offset with tuned α vs. measured, ‰	1.224	-1.230

Table S5. CO mole fraction, ^{14}CO measurements, and estimates of in-situ cosmogenic ^{14}CO content in the large volume samples and field procedural blanks. All errors presented indicate the 95% confidence interval

Sample name	CO measured (nmol/mol)	^{14}CO measured (pMC)	^{14}CO corrected for dilution with 10 µmol/mol [CO] ^{14}C-depleted gas		^{14}CO corrected for procedural blanks	Cosmogenic ^{14}CO after corrections
			(pMC)	(molec/cc STP)	(molec/cc STP)	(molec/per g ice)**
SFC	166.3 ± 5.9	88.1 ± 2.0	7541 ± 383	394.5 ± 14.2	371.3 ± 14.7	36.7 ± 2.3
19.5m	166.7 ± 5.8	67.0 ± 0.8	5732 ± 266	300.5 ± 9.2	277.3 ± 9.7	23.7 ± 1.4
30m	2149.1 ± 5.9	60.9 ± 0.9	415 ± 12	280.6 ± 8.3	257.4 ± 8.8	23.9 ± 1.8
40.5m	179.8 ± 5.8	35.0 ± 0.5	3419 ± 156	193.4 ± 6.2	170.2 ± 6.9	15.7 ± 1.0
51m	208.0 ± 5.9	98.8 ± 1.0	2485 ± 96	162.6 ± 4.5	139.4 ± 5.5	13.1 ± 0.9
61.5m	117.8 ± 5.9	88.5 ± 1.0	3835 ± 216	142.0 ± 4.0	118.9 ± 5.1	11.2 ± 0.7
72m	110.0 ± 5.8	82.7 ± 0.9	3845 ± 227	133.0 ± 3.8	109.8 ± 5.0	10.7 ± 0.7
^{14}C dead blank 1	40.1 ± 6.0	19.0 ± 0.5	1919 ± 294	24.1 ± 0.9		
^{14}C dead blank 2	41.7 ± 5.8	16.3 ± 0.3	1562 ± 226	20.4 ± 0.7		
^{14}C modern blank 1	40.1 ± 5.9	19.0 ± 0.4	1774 ± 272	22.2 ± 0.8		
^{14}C modern blank 2	42.0 ± 5.9	8.9 ± 0.2	1758 ± 261	23.1 ± 1.1		
^{14}C dead dilution gas	10020 ± 130	0.17 ± 0.6				

**this sample yielded an anomalously high CO mole fraction, indicating some form of contamination*
***includes the solubility correction for CO mole fraction because CO is slightly more soluble than air*

Table S6. $^{14}CH_4$ corrections for the large volume samples. All errors presented indicate the 95% confidence interval.

Sample name	Measured $^{14}CH_4$	$^{14}CH_4$ corrected for processing blanks		$^{14}CH_4$ amount per gram ice
	(pMC)	*(pMC)*	*(molec/cc STP)*	*(molec/g ice)*
Sfc sample	61.1 ± 2.2	62.7 ± 2.5	8.555 ± 0.357	0.840 ± 0.054
19.5m	15.4 ± 0.6	15.4 ± 0.7	2.270 ± 0.144	0.193 ± 0.016
30m	13.9 ± 0.6	13.9 ± 0.7	2.322 ± 0.152	0.214 ± 0.020
40.5m	10.1 ± 0.4	9.9 ± 0.5	1.284 ± 0.122	0.118 ± 0.013
51m	7.0 ± 0.5	6.7 ± 0.5	1.031 ± 0.133	0.096 ± 0.013
61.5m	5.4 ± 0.4	5.0 ± 0.5	0.831 ± 0.127	0.078 ± 0.013
72m	5.9 ± 0.4	5.5 ± 0.5	0.817 ± 0.124	0.079 ± 0.013
^{14}C dead blank 1	0.8 ± 0.1			
^{14}C dead blank 2	1.0 ± 0.1			
^{14}C modern blank 1	132.9 ± 1.6			
^{14}C modern blank 2	132.5 ± 1.6			
^{14}C dead “true”	0.31 ± 0.03			
^{14}C modern “true”	137.2 ± 1.4			

Table S7. Measured ^{14}C activities of commensurately-sized ^{14}C standards and their expected ^{14}C activities. The 50µg and standard 15µg set are used to empirically correct the ^{14}CO and $^{14}CO_2$ sample pMC values, respectively (Fig. S1a and S1b). The measured ^{14}C activities are corrected for $\delta^{13}C$ and the errors represent 68% (1σ) confidence interval. The expected ^{14}C activity of the OxII standard is based on consensus value reported by Wacker et al. (2019). The expected ^{14}C activities of the IAEA-C7 and C8 standard are based on values reported by Le Clercq et al. (1997). Finally, the expected ^{14}C activities of ANSTO internal "dead CO_2" and L733 standard are based on large (1mg) samples graphitized with the ANSTO conventional furnaces (Hua et al., 2004).

Sample name	Measured ^{14}C activity (pMC)	Error (pMC)	Expected ^{14}C activity (pMC)	Error (pMC)
50 µg set (^{14}CO sample set)				
Dead CO2	0.20	0.03		
Dead CO2	0.15	0.03	0.03	0.02
Dead CO2	0.17	0.03		
STD OxII	134.90	0.48		
STD OxII	133.31	0.61	134.06	0.08
STD OxII	134.93	0.60		
IAEA-C7	49.89	0.29	49.53	0.24
IAEA-C7	50.09	0.33		
STD L733	86.83	0.36	86.27	0.53
STD L733	87.51	0.43		
15 µg set ($^{14}CO_2$ sample set)				
Dead CO2	0.41	0.05		
Dead CO2	0.45	0.20	0.03	0.02
Dead CO2	0.36	0.11		
Dead CO2	0.40	0.06		
STD OxII	134.96	0.85		
STD OxII	134.54	0.82	134.06	0.08
STD OxII	133.23	0.80		
STD OxII	133.33	0.72		
IAEA-C7	49.99	0.47	49.53	0.24
IAEA-C8	14.99	0.27	15.03	0.34
STD L733	83.81	0.55	86.27	0.53

Table S8. $^{14}CO_2$ measurements on laboratory-made bubble-free ice (BFI) samples, including measured ^{14}C, ^{14}C corrected for ANSTO processing, measured carbon mass (M_g), expected carbon mass (M_s), extraneous carbon mass (M_{ext}), and calculated ^{14}C activity of extraneous carbon. The "true" $^{14}CO_2$ activities for the standard gases are 102.48 ± 0.42 and 0.38 ± 0.06 pMC for the "modern" and "dead" standards respectively. All errors presented indicate the 95% confidence interval.

Standard gas used	Measured $^{14}CO_2$	$^{14}CO_2$ corrected for ANSTO processing ($^{14}C_g$)	M_g	M_s	M_{ext}	^{14}C activity of extraneous C ($^{14}C_{ext}$)
	(pMC)	*(pMC)*	*(µg)*	*(µg)*	*(µg)*	*(pMC)*
Modern	102.5 ± 1.6	102.7 ± 2.2	12.3 ± 0.2	11.8 ± 0.2	0.5 ± 0.3	108.5 ± 141.2
Modern	103.0 ± 1.4	103.2 ± 2.0	12.0 ± 0.2	11.7 ± 0.2	0.3 ± 0.3	130.8 ± 222.5
Modern	104.7 ± 1.4	104.9 ± 2.0	11.9 ± 0.2	11.6 ± 0.2	0.3 ± 0.3	198.3 ± 268.4
Dead	3.9 ± 0.4	3.7 ± 1.0	11.7 ± 0.2	11.4 ± 0.2	0.3 ± 0.3	111.9 ± 105.7
Dead	3.8 ± 0.4	3.6 ± 1.0	13.3 ± 0.2	13.0 ± 0.3	0.4 ± 0.3	122.9 ± 127.0
Dead	3.2 ± 0.4	3.0 ± 1.0	13.5 ± 0.2	13.2 ± 0.3	0.3 ± 0.3	116.4 ± 140.3
Dead	3.2 ± 0.3	3.0 ± 1.0	13.1 ± 0.2	12.7 ± 0.3	0.3 ± 0.3	104.7 ± 114.9
Modern	100.7 ± 1.3	101.0 ± 1.9	14.2 ± 0.2	13.9 ± 0.2	0.4 ± 0.3	44.2 ± 163.2
Modern	103.6 ± 1.5	103.9 ± 2.1	12.0 ± 0.2	11.8 ± 0.2	0.2 ± 0.3	195.0 ± 461.3
				Average (n=9)		**125.9**
				Standard deviation		**94.2**
				Standard error		**31.4**

Table S9. $^{14}CO_2$ measurements, CO_2 mole fraction measurements, total air content (TAC), corrections, and error-propagated uncertainties. Most samples, with the exception of the ones with *next to their depths were collected from 2015/16 deep borehole #2. All errors presented indicate the 95% confidence interval.

Depth	Measured ^{14}C	CO_2 mole fraction	^{14}C corrected for ANSTO processing ($^{14}C_g$)	Measured mass (M_g)	Expected mass (M_s)	Extraneous mass M_{ext}	^{14}C corrected for extraneous C ($^{14}C_s$)		Total air content	^{14}C corrected for postcoring ^{14}C production
(m)	*(pMC)*	*(nmol/mol)*	*(pMC)*	*(µg)*	*(µg)*	*(µg)*	*(pMC)*	*(molec/g ice)*	*cc STP/g ice*	*(molec/g ice)*
2.25	31.0 ± 0.8	208.69 ± 1.81	30.9 ± 1.2	13.1 ± 0.2	12.6 ± 0.4	0.5 ± 0.5	27.1 ± 5.1	153.7 ± 29.0	0.0839 ± 0.0005	145.5 ± 32.0
2.25	27.6 ± 1.2		27.5 ± 1.5	12.6 ± 0.2	12.0 ± 0.3	0.5 ± 0.4	23.2 ± 4.4	131.4 ± 24.9		123.3 ± 28.5
3.65	19.4 ± 0.7	208.19 ± 1.81	19.3 ± 1.1	13.6 ± 0.2	13.0 ± 0.3	0.6 ± 0.4	14.3 ± 4.3	96.7 ± 28.8	0.1001 ± 0.0007	88.5 ± 31.9
3.65	18.9 ± 0.9		18.7 ± 1.2	13.3 ± 0.2	13.0 ± 0.3	0.4 ± 0.4	15.7 ± 4.1	106.2 ± 27.9		98.0 ± 31.1
5.25	17.8 ± 0.7	212.56 ± 1.81	17.7 ± 1.1	13.3 ± 0.2	12.9 ± 0.3	0.4 ± 0.4	14.0 ± 4.1	98.8 ± 28.6	0.1022 ± 0.0007	90.6 ± 31.8
5.25	18.4 ± 0.6		18.3 ± 1.0	13.8 ± 0.2	13.3 ± 0.3	0.5 ± 0.4	14.6 ± 4.1	103.0 ± 28.8		94.8 ± 31.9
6.85	14.2 ± 0.7	212.31 ± 1.81	14.1 ± 1.1	12.7 ± 0.2	12.3 ± 0.3	0.4 ± 0.4	10.4 ± 4.1	72.4 ± 28.3	0.1015 ± 0.0004	64.2 ± 31.6
6.85	14.4 ± 0.6		14.2 ± 1.0	12.8 ± 0.2	12.5 ± 0.3	0.3 ± 0.4	11.1 ± 4.0	77.6 ± 28.1		69.4 ± 31.3
10	13.4 ± 0.6	214.98 ± 1.81	13.3 ± 1.0	12.8 ± 0.2	12.4 ± 0.3	0.5 ± 0.4	8.9 ± 4.1	58.8 ± 26.9	0.0946 ± 0.0004	50.6 ± 30.3
10	13.2 ± 0.7		13.1 ± 1.1	13.0 ± 0.2	12.6 ± 0.3	0.4 ± 0.4	9.5 ± 4.1	62.5 ± 26.7		54.3 ± 30.0
15*	13.7 ± 0.8	220.65 ± 1.81	13.6 ± 1.2	11.6 ± 0.2	11.2 ± 0.3	0.3 ± 0.3	10.2 ± 4.0	69.1 ± 27.4	0.0952 ± 0.0007	60.9 ± 30.7
15*	12.2 ± 0.6		12.0 ± 1.0	10.3 ± 0.2	10.1 ± 0.2	0.2 ± 0.3	9.2 ± 3.9	62.8 ± 26.7		54.6 ± 30.2
19.5	12.0 ± 0.5	221.37 ± 1.81	11.9 ± 1.0	10.7 ± 0.2	10.6 ± 0.2	0.1 ± 0.3	10.3 ± 3.9	60.5 ± 22.9	0.0821 ± 0.0004	52.4 ± 26.6
19.5	11.8 ± 0.7		11.6 ± 1.1	11.9 ± 0.2	11.7 ± 0.3	0.2 ± 0.3	9.8 ± 3.9	57.8 ± 22.9		49.6 ± 26.7
30**	13.1 ± 0.6	223.22 ± 1.81	12.9 ± 1.0	13.9 ± 0.2	13.6 ± 0.5	0.3 ± 0.6	10.2 ± 5.8	67.4 ± 38.3	0.0918 ± 0.0007	59.2 ± 40.8
40.5	9.0 ± 0.5	231.71 ± 1.81	8.8 ± 1.0	11.8 ± 0.2	11.6 ± 0.3	0.2 ± 0.3	6.7 ± 4.0	44.6 ± 26.5	0.0887 ± 0.0007	36.4 ± 29.9
40.5	10.4 ± 0.5		10.3 ± 1.0	12.3 ± 0.2	11.9 ± 0.3	0.4 ± 0.3	6.8 ± 3.9	45.4 ± 26.0		37.2 ± 29.5
51	8.7 ± 0.5	227.75 ± 1.81	8.5 ± 1.0	13.2 ± 0.2	12.9 ± 0.3	0.3 ± 0.4	5.5 ± 3.9	39.3 ± 27.7	0.0965 ± 0.0002	31.1 ± 30.9
51*	8.5 ± 0.7	229.17 ± 1.81	8.3 ± 1.1	14.5 ± 0.2	14.1 ± 0.3	0.4 ± 0.4	5.2 ± 3.9	36.2 ± 27.4	0.0940 ± 0.0004	28.0 ± 30.6
61.5	8.2 ± 0.4	239.82 ± 1.81	8.1 ± 0.9	14.3 ± 0.2	14.0 ± 0.3	0.3 ± 0.4	5.2 ± 3.8	39.2 ± 28.5	0.0961 ± 0.0005	31.0 ± 31.8
61.5*	7.4 ± 0.4	238.35 ± 1.81	7.3 ± 0.9	14.2 ± 0.2	13.8 ± 0.3	0.3 ± 0.4	4.3 ± 3.8	30.3 ± 27.0	0.0918 ± 0.0002	22.1 ± 30.3
72	7.2 ± 0.4	239.92 ± 1.81	7.0 ± 0.9	12.4 ± 0.2	12.0 ± 0.3	0.4 ± 0.3	2.7 ± 3.9	20.0 ± 29.2	0.0960 ± 0.0003	11.8 ± 32.4
72	7.0 ± 0.4		6.8 ± 0.9	13.4 ± 0.2	13.0 ± 0.3	0.4 ± 0.4	2.9 ± 3.9	21.7 ± 29.0		13.6 ± 32.1

*these samples were collected from borehole #3
**replicate sample was lost

Table S10. $^{14}CO_2$ measurements corrected for ANSTO processing, CO_2 mole fraction, and "total air content" of the laboratory-produced and field-produced BFI samples that were run with the ^{14}C-dead standard. The CO_2 mole fraction in the BFI samples was determined from the ratio of the amount of CO_2 and air collected, measured in the manometers. The "air content" of the BFI samples was determined from the ratio of the amount of air collected in the manometer and the amount of bubble-free-ice sublimated. All errors presented indicate the 95% confidence interval.

Sample Name	**^{14}C corrected for ANSTO processing** *(pMC)*	**CO_2 mole fraction** *(µmol/mol)*	**"Air content"** *(ccSTP/g ice)*	**$^{14}CO_2$ content** *(molecule/g ice)*
Field#1	3.8 ± 0.5	308.3 ± 4.0	0.096 ± 0.007	34.5 ± 11.6
Field#5	2.5 ± 0.5	306.7 ± 4.0	0.100 ± 0.007	23.4 ± 10.6
Field#4	4.3 ± 0.6	308.9 ± 4.0	0.074 ± 0.007	30.5 ± 10.0
Field#2	4.2 ± 0.5	313.0 ± 4.1	0.074 ± 0.007	30.1 ± 9.4
Lab#5	3.7 ± 0.5	310.8 ± 4.1	0.071 ± 0.007	24.8 ± 8.7
Lab#6	3.6 ± 0.5	309.8 ± 4.0	0.070 ± 0.007	24.1 ± 8.4
Lab#8	3.0 ± 0.5	308.6 ± 4.0	0.070 ± 0.007	19.9 ± 7.9
Lab#9	3.0 ± 0.5	309.4 ± 4.0	0.059 ± 0.007	16.9 ± 6.5
		Average field ± stdev		**29.7 ± 4.6**
		Average lab ± stdev		**21.4 ± 3.7**
		Average postcoring ± stdev		**8.2 ± 5.9**

REFERENCES

Baggenstos, D., Bauska, T. K., Severinghaus, J. P., Lee, J. E., Schaefer, H., Buizert, C., Brook, E. J., Shackleton, S., and Petrenko, V. V.: Atmospheric gas records from Taylor Glacier, Antarctica, reveal ancient ice with ages spanning the entire last glacial cycle, 13, 943, 2017.

Balco, G., Stone, J. O., Lifton, N. A., and Dunai, T. J.: A complete and easily accessible means of calculating surface exposure ages or erosion rates from 10Be and 26Al measurements, 3, 174–195, 2008.

Bereiter, B., Eggleston, S., Schmitt, J., Nehrbass-Ahles, C., Stocker, T. F., Fischer, H., Kipfstuhl, S., and Chappellaz, J.: Revision of the EPICA Dome C CO2 record from 800 to 600 kyr before present, Geophys. Res. Lett., 42, 2014GL061957, https://doi.org/10.1002/2014GL061957, 2015.

Chappellaz, J., Stowasser, C., Blunier, T., Baslev-Clausen, D., Brook, E. J., Dallmayr, R., Faïn, X., Lee, J. E., Mitchell, L. E., and Pascual, O.: High-resolution glacial and deglacial record of atmospheric methane by continuous-flow and laser spectrometer analysis along the NEEM ice core, 9, 2579–2593, 2013.

Clercq, M. L., Plicht, J. V. D., and Gröning, M.: New 14C Reference Materials with Activities of 15 and 50 pMC, 40, 295–297, https://doi.org/10.1017/S0033822200018178, 1997.

Hua, Q., Zoppi, U., Williams, A. A., and Smith, A. M.: Small-mass AMS radiocarbon analysis at ANTARES, Nuclear Instruments and Methods in Physics Research Section B: Beam Interactions with Materials and Atoms, 223–224, 284–292, https://doi.org/10.1016/j.nimb.2004.04.057, 2004.

Loulergue, L., Schilt, A., Spahni, R., Masson-Delmotte, V., Blunier, T., Lemieux, B., Barnola, J.-M., Raynaud, D., Stocker, T. F., and Chappellaz, J.: Orbital and millennial-scale features of atmospheric CH 4 over the past 800,000 years, 453, 383, 2008.

McNaught, A. D. and Wilkinson, A.: Compendium of chemical terminology, Blackwell Science Oxford, 1997.

Mitchell, L., Brook, E., Lee, J. E., Buizert, C., and Sowers, T.: Constraints on the Late Holocene Anthropogenic Contribution to the Atmospheric Methane Budget, *Science*, **342**, 964–966, 2013.

Menking, J. A., Brook, E. J., Shackleton, S. A., Severinghaus, J. P., Dyonisius, M. N., Petrenko, V., McConnell, J. R., Rhodes, R. H., Bauska, T. K., and Baggenstos, D.: Spatial pattern of accumulation at Taylor Dome during Marine Isotope Stage 4: stratigraphic constraints from Taylor Glacier, *Clim. Past.*, **15**, 1537–1556, 2019.

Mitchell, L. E., Brook Edward J., Sowers Todd, McConnell J. R., and Taylor Kendrick: Multidecadal variability of atmospheric methane, 1000–1800 C.E., Journal of Geophysical Research: Biogeosciences, 116, https://doi.org/10.1029/2010JG001441, 2011.

Petrenko, V. V., Severinghaus, J. P., Brook, E. J., Reeh, N., and Schaefer, H.: Gas records from the West Greenland ice margin covering the Last Glacial Termination: a horizontal ice core,

Quaternary Science Reviews, 25, 865–875, https://doi.org/10.1016/j.quascirev.2005.09.005, 2006.

Petrenko, V. V., Smith, A. M., Brailsford, G., Riedel, K., Hua, Q., Lowe, D., Severinghaus, J. P., Levchenko, V., Bromley, T., Moss, R., Mühle, J., and Brook, E. J.: A New Method for Analyzing 14C of Methane in Ancient Air Extracted from Glacial Ice, 50, 53–73, https://doi.org/10.2458/azu_js_rc.50.3033, 2008.

Petrenko, V. V., Severinghaus, J. P., Schaefer, H., Smith, A. M., Kuhl, T., Baggenstos, D., Hua, Q., Brook, E. J., Rose, P., Kulin, R., Bauska, T., Harth, C., Buizert, C., Orsi, A., Emanuele, G., Lee, J. E., Brailsford, G., Keeling, R., and Weiss, R. F.: Measurements of 14C in ancient ice from Taylor Glacier, Antarctica constrain in situ cosmogenic 14CH4 and 14CO production rates, Geochimica et Cosmochimica Acta, 177, 62–77, https://doi.org/10.1016/j.gca.2016.01.004, 2016.

Rasmussen S. O., Andersen K. K., Svensson A. M., Steffensen J. P., Vinther B. M., Clausen H. B., Siggaard-Andersen M.-L., Johnsen S. J., Larsen L. B., Dahl-Jensen D., Bigler M., Röthlisberger R., Fischer H., Goto-Azuma K., Hansson M. E., and Ruth U.: A new Greenland ice core chronology for the last glacial termination, Journal of Geophysical Research: Atmospheres, 111, https://doi.org/10.1029/2005JD006079, 2006.

Rasmussen, S. O., Abbott, P. M., Blunier, T., Bourne, A. J., Brook, E., Buchardt, S. L., Buizert, C., Chappellaz, J., Clausen, H. B., Cook, E., Dahl-Jensen, D., Davies, S. M., Guillevic, M., Kipfstuhl, S., Laepple, T., Seierstad, I. K., Severinghaus, J. P., Steffensen, J. P., Stowasser, C., Svensson, A., Vallelonga, P., Vinther, B. M., Wilhelms, F., and Winstrup, M.: A first chronology for the North Greenland Eemian Ice Drilling (NEEM) ice core, Clim. Past, 9, 2713–2730, https://doi.org/10.5194/cp-9-2713-2013, 2013.

Turney, C., Fogwill, C., Van Ommen, T. D., Moy, A. D., Etheridge, D., Rubino, M., Curran, M. A., and Rivera, A.: Late Pleistocene and early Holocene change in the Weddell Sea: a new climate record from the Patriot Hills, Ellsworth Mountains, West Antarctica, 28, 697–704, 2013.

Shackleton, S., Baggenstos, D., Menking, J. A., Dyonisius, M. N., Bereiter, B., Bauska, T. K., Rhodes, R. H., Brook, E. J., Petrenko, V. V., McConnell, J. R., Kellerhals, T., Häberli, M., Schmitt, J., Fischer, H., and Severinghaus, J. P.: Global ocean heat content in the Last Interglacial, *Nat. Geosci.*, **13**, 77–81, 2020.

van De Wal, R. S. W., Meijer, H. a. J., De Rooij, M., and Van Der Veen, C.: Radiocarbon analyses along the EDML ice core in Antarctica, *Tellus. B*, **59**, 157–165, 2007.

van der Kemp, W. J. M., Alderliesten, C., Van der Borg, K., Holmlund, P., de Jong, A. F. M., Karlöf, L., Lamers, R. A. N., Oerlemans, J., Thomassen, M., and Van de Wal, R. S. W.: Very little in situ produced radiocarbon retained in accumulating Antarctic ice, *Nucl. Instrum. Meth. B*, **172**, 632–636, 2000.

Veres, D., Bazin, L., Landais, A., Toyé Mahamadou Kele, H., Lemieux-Dudon, B., Parrenin, F., Martinerie, P., Blayo, E., Blunier, T., and Capron, E.: The Antarctic ice core chronology (AICC2012): an optimized multi-parameter and multi-site dating approach for the last 120 thousand years, 9, 1733–1748, 2013.

Wacker, L., Bollhalder, S., Sookdeo, A., and Synal, H.-A.: Re-evaluation of the New Oxalic Acid standard with AMS, Nuclear Instruments and Methods in Physics Research Section B: Beam Interactions with Materials and Atoms, 455, 178–180, https://doi.org/10.1016/j.nimb.2018.12.035, 2019.